Journal of Power Sources 186 (2009) 485–489

Contents lists available at ScienceDirect

Journal of Power Sources

journal homepage: www.elsevier.com/locate/jpowsour

Short communication

Synthesis and electrochemical properties of LSM and LSF perovskites as anode materials for high temperature steam electrolysis

Jiangrong Kong[a,b,*], Yong Zhang[a,b,**], Changsheng Deng[a,b], Jingming Xu[a]

[a] Institute of Nuclear and New Energy Technology, Tsinghua University, Beijing 100084, PR China
[b] State Key Laboratory of New Ceramics and Fine Processing, Beijing 100084, PR China

ARTICLE INFO

Article history:
Received 28 August 2008
Received in revised form 9 October 2008
Accepted 10 October 2008
Available online 1 November 2008

Keywords:
High temperature steam electrolysis (HTSE)
Solid oxide electrolysis cell (SOEC)
Sol–gel self-propagating
Composite anode
Electrochemical performance

ABSTRACT

$La_{0.8}Sr_{0.2}MnO_3$ (LSM) and $La_{0.8}Sr_{0.2}FeO_3$ (LSF) perovskites used as the anode materials for high temperature steam electrolysis (HTSE) were synthesized by sol–gel self-propagating method. These two powders were mixed with yttria-stabilized zirconia (YSZ) powders, respectively to fabricate composite anodes of solid oxide electrolysis cells (SOECs). The LSM–YSZ and LSF–YSZ composite anodes were tested at 1073 K SOEC working temperature under electrolysis conditions, using cells with a YSZ electrolyte and a Pt counter electrode. Their electrochemical performances were compared and the possibilities of using as SOEC anodes were discussed.

1. Introduction

Hydrogen is regarded as a leading candidate for alternative future fuels [1]. It has the potential to address the environmental and energy security issues associated with fossil-derived hydrocarbon fuels [2]. However, many processing challenges need to be met before hydrogen can be widely used. Recently hydrogen production efficiency was evaluated in the process coupling with nuclear energy. High temperature steam electrolysis (HTSE) utilizes the heat and electricity energy of the high temperature gas-cooled reactor (HTGR) as the energy sources of solid oxide electrolysis cell (SOEC), which is a promising method for highly efficient large-scale hydrogen production [3–5].

The SOEC approach was based on existing materials and fabrication technology developed for planar solid oxide fuel cells (SOFC) [6–10]. The current investigations focus on hydrogen production efficiency, relationships between macroscopic parameters, dynamic models and so on [11–13]. Although there have been extensive investigations into electrocatalysis mechanisms in SOFC, relatively few studies have been published on SOEC.

Because air electrode is often the limiting component for SOFC operating on H_2, a more detailed investigation on SOEC anode is needed to improve its performance and efficiency [14]. The objective of our work is to find a suitable material and use it to prepare composite anodes with lower overpotentials, reduced polarization and interface resistances, and improved electrode reaction mechanism.

So far, the most commonly used anode materials for SOECs is a composite of yttria-stabilized zirconia (YSZ) and strontium-doped lanthanum manganites (LSM), which is the common material used in high-temperature and intermediate temperature SOFC (IT-SOFC) cathodes. In addition, Sr doped $LaFeO_3$ (LSF) has a relatively low thermal expansion coefficient (TEC) and a high compatibility with zirconia based electrolyte. Owning a favorable electron characteristic and an admirable thermal stability, it was utilized as IT-SOFC cathode material [15]. To help improving the electrochemical catalytic behavior, the use of LSF as SOEC anode material was attempted in this paper.

In this paper, two kinds of perovskites $La_{0.8}Sr_{0.2}MnO_3$ (LSM20) and $La_{0.8}Sr_{0.2}FeO_3$ (LSF20) were synthesized by sol–gel self-propagating method. LSM–YSZ and LSF–YSZ composite anodes were fabricated on YSZ electrolyte discs and their electrochemical properties and thermo-cyclic stabilities were investigated. The possibilities of their applications in HTSE were discussed as well.

* Corresponding author at: Institute of Nuclear and New Energy Technology, Tsinghua University, Beijing 100084, PR China. Tel.: +86 10 80194017; fax: +86 10 89796022.
** Co-corresponding author.
E-mail addresses: kongjr@mail.tsinghua.edu.cn (J. Kong), yzhang@mail.tsinghua.edu.cn (Y. Zhang).

0378-7753/$ – see front matter © 2008 Elsevier B.V. All rights reserved.
doi:10.1016/j.jpowsour.2008.10.053

2. Experimental

2.1. Synthesis of perovskite powders

Perovskite powders LSM20 and LSF20 were synthesized by sol–gel self-propagating method. Lanthanum nitrate ($La(NO_3)_3{\cdot}6H_2O$, AR), strontium nitrate ($Sr(NO_3)_2$, AR), manganous nitrate ($Mn(NO_3)_2$, 50% aqueous solution, AR) and ferric nitrate ($Fe(NO_3)_3{\cdot}9H_2O$, AR) were used as raw materials, respectively. The nitrates in proper ratio were dissolved in deionized water, and citric acid was added in equal molar ratio. The above solution was mixed at 353 K under constant stirring and the pH value of the solution was adjusted to 7 with ammonia. Then, a homogenous clear sol solution was achieved. The sol solution was heated to condense and the sol transformed into a dried gel. After that, the dried gel precursor was put in a furnace and was ignited. The self-propagation was initiated and spread rapidly in the whole system and the combustion was finished instantaneously. The as-burned loose powders were treated at 1073 K to make the incompletely combusted part react thoroughly. The target perovskite oxide powder was then obtained.

2.2. Preparations of SOEC composite anodes and three-electrode system

The obtained LSM20 and LSF20 powders were mixed with YSZ powders (Tosoh, Japan) and organic binder to make screen-printing paste, respectively. Discs of YSZ with a thickness of 500 μm and a diameter of 16 mm were used as solid electrolyte. The LSM–YSZ and LSF–YSZ pastes were screen printed onto the YSZ electrolyte discs and sintered at 1473 K for 2 h. Then, LSM20–YSZ/YSZ and LSF20–YSZ/YSZ composite anode/electrolyte half-cells were obtained. Subsequently, Pt paste was screen-printed alongside of the anode (work electrode, WE) as the reference electrode (RE) and onto the other side of the YSZ electrolyte disc as the counter electrode (CE), respectively. Pt wires were stuck on the anode, the RE and the CE, respectively. Pt paste was solidified at 850 °C for 10 min in air. The three-electrodes are schematically shown in Fig. 1.

2.3. Characterization

The crystal structures of the synthesized powders were determined by X-ray diffraction (XRD) using Cu K_α radiation. The morphology of synthesized powders was examined by transmission electron microscope (TEM).

An Im6ex (Zahner, Germany) electrochemical workstation was employed for anodic polarization and electrochemical impedance spectroscopy (EIS) measurements. The Electrochemical impedance measurements were performed in the frequency range of 100 kHz–100 mHz with an applied amplitude of 5 mV under open circuit at 800 °C. The measured spectra were fitted to the equivalent circuit with the nonlinear least square fitting software, ZSimpWin.

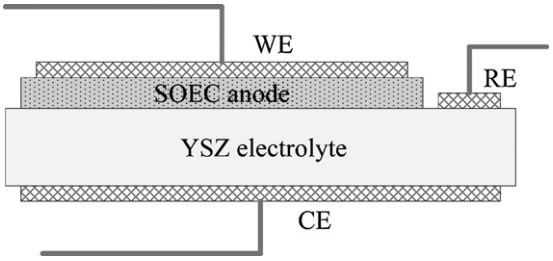

Fig. 1. Schematic of three-electrode system.

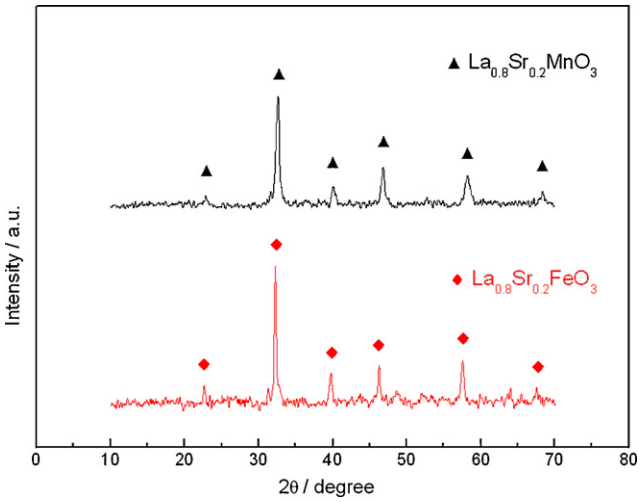

Fig. 2. XRD patterns of LSM20 and LSF20 powders synthesized by sol–gel self-propagating method.

3. Results and discussion

3.1. Phase formation

Fig. 2 shows the XRD patterns of LSM20 and LSF20, respectively. Compared with X-ray diffraction pattern JCPDS, the powders were pure single phase.

3.2. Morphology of synthesized powders

Figs. 3 and 4 show the TEM images of LSM20 and LSF20 perovskite powders, respectively. Both micrographs show agglomerates made up of smaller particles. The particle size of LSM20 was about 30 nm, while that of LSF20 is larger with size of 40 nm. The LSF20 powders had almost spherical shape, while the LSM20 powders had sharp edges and irregular shape.

3.3. Microstructure of SOEC composite anodes

The microstructure of an electrode has great influence on its electrochemical performance. High porosity promotes the gas

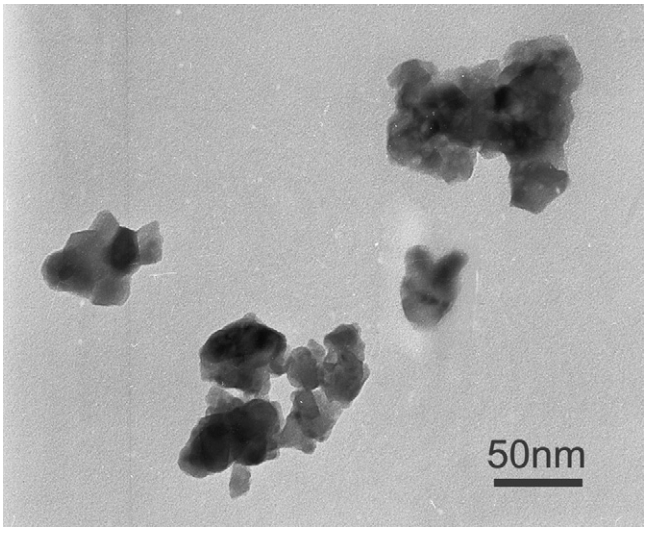

Fig. 3. TEM image of LSM20 powder synthesized by sol–gel self-propagating method.

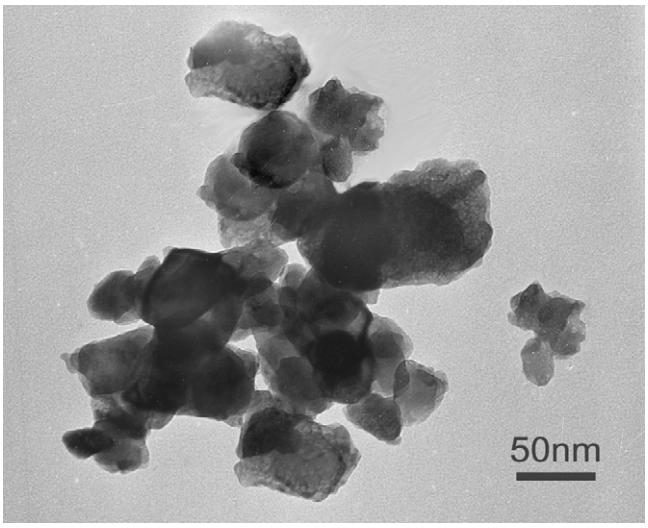

Fig. 4. TEM image of LSF20 powder synthesized by sol–gel self-propagating method.

transport in the gas diffusion electrode. Close contact between the electrode and the electrolyte materials is in favor of the formation of triple-phase boundary (TPB). SEM images of LSM20–YSZ and LSF20–YSZ composite anodes are given in Figs. 5 and 6, respectively. It is found from the cross-section of electrolyte/electrode images (Figs. 5a and 6a) that the thicknesses of the two type composite anodes were 30–40 μm. The electrode layer combined closely with the electrolyte and almost no defects were observed. In addition, the grain size of LSM20–YSZ composite anode is finer than that of LSF20–YSZ, while the porosity of LSF20–YSZ is relatively larger than that of LSM20–YSZ. Moreover, it is shown in magnified images of electrode bulk (Figs. 5b and 6b) that the LSM20 grains had a loose adhesion with YSZ ceramic skeletons while LSF20 grains had a close contact. It is demonstrated that for both composite anodes the two phases were well distributed and the YSZ grains appeared to be interconnected.

3.4. Electrochemical performance of SOEC composite anodes

The SOEC working temperature was 1073 K. Both composite anodes, after electrochemical tests at 1073 K, were cooled down to room temperature. After that, the temperature was raised back to 1073 K and another electrochemical measurement was taken. That is to say, the second electrochemical test was taken after a complete thermal cycle. A preliminary evaluation of the thermo-cyclic stabilities could be made according to the difference between the results of the two tests.

Polarization performance is a main sign of an electrode performance. Liner potentiodynamic sweep was adopted in this work. The potential scan-range was 0–0.3 V. And the sweep rate was 5 mV s^{-1}. The anodic polarization curves of LSM20–YSZ and LSF20–YSZ composite anodes are shown in Fig. 7. The current densities of

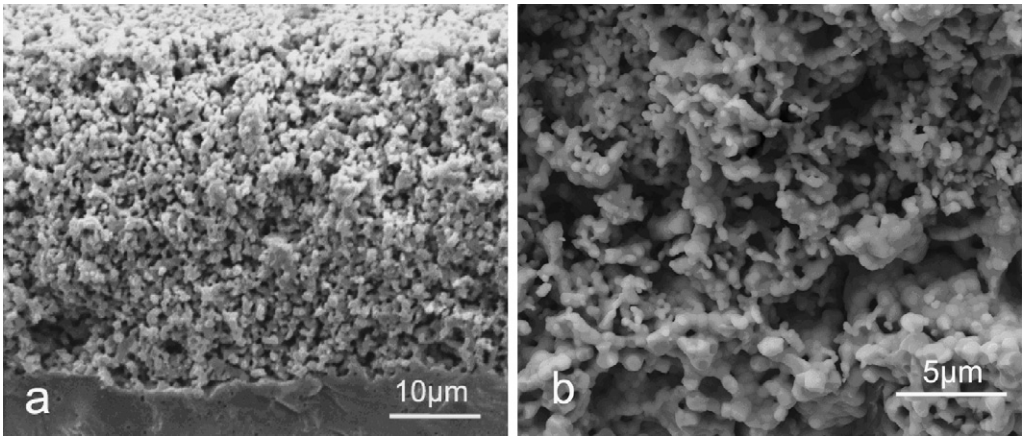

Fig. 5. Scanning electron micrographs of LSM20–YSZ composite anode (a) cross-section of electrolyte/anode; (b) magnified image of anode bulk).

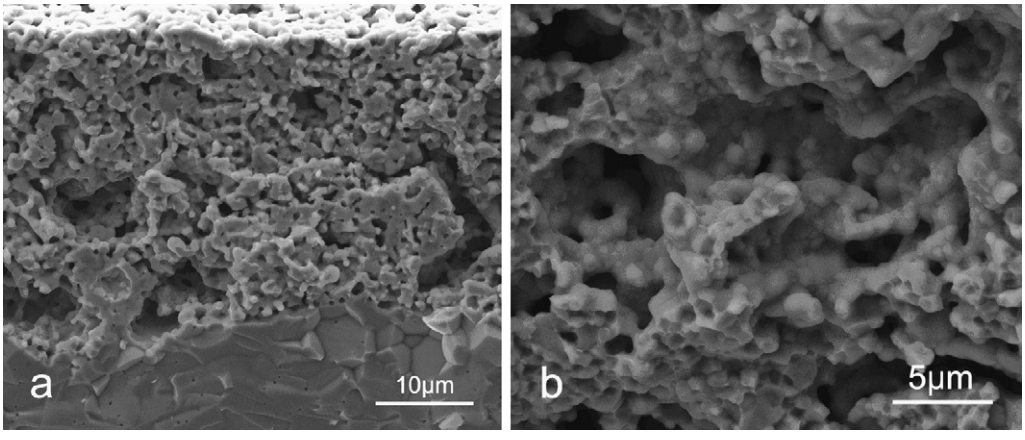

Fig. 6. Scanning electron micrographs of LSF20–YSZ composite anode (a) cross-section of electrolyte/anode; (b) magnified image of anode bulk).

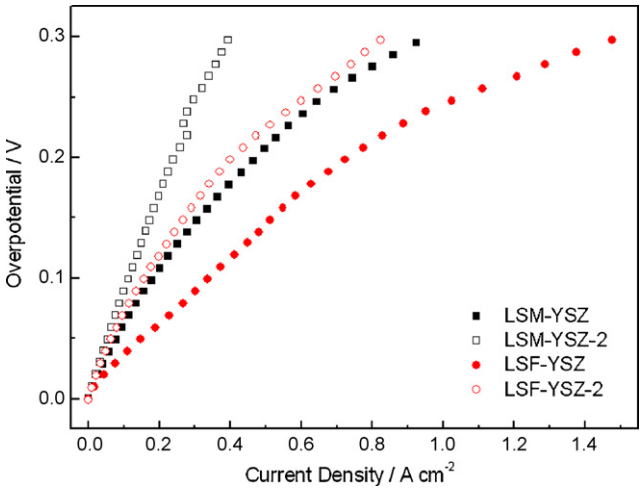

Fig. 7. Anodic polarization curves of LSM20–YSZ and LSF20–YSZ at 1073 K (■: LSM20–YSZ before thermal cycling, ●: LSF20–YSZ before thermal cycling, □: LSM20–YSZ after thermal cyclic treatment, ○: LSF20–YSZ after thermal cyclic treatment).

LSM20–YSZ anode at 0.1 V overpotential were 0.1776 A cm^{-2} and 0.1124 A cm^{-2} before and after thermocycling, respectively. The current densities of LSF20–YSZ anode at 0.1 V overpotential were 0.3360 A cm^{-2} and 0.1560 A cm^{-2} before and after thermocycling, respectively. At the same overpotential, the current density of LSF20–YSZ anode was larger than that of the LSM20–YSZ anode. The current densities of both anodes were decreased after a complete thermal cycle, indicating electrode degradations.

The electrochemical behavior of the composite anodes was investigated by EIS measurements under open circuit conditions contemporary with anodic polarization tests. Fig. 8 shows Nyquist plots of the composite anodes at open circuit voltage (OCV) tested at 1073 K. The spectra were fitted with the ZSimpWin program, and the equivalent circuit diagram is also given in Fig. 8. The physical parameters were denoted as follows: R_s is the ohmic resistance of electrolyte and lead wires, R_{ct} is charge-transfer resistance, *CPE* (Q) is the constant phase element, and L is the inductance of lead wires.

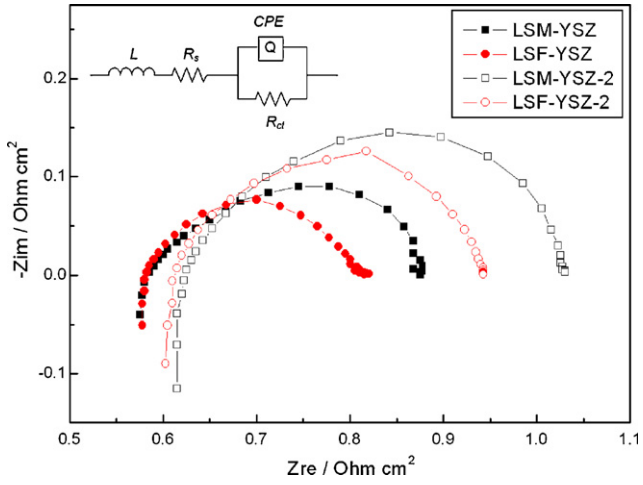

Fig. 8. Nyquist plots and equivalent circuit diagram of LSM20–YSZ and LSF20–YSZ composite anodes at OCV tested at 1073 K (■: LSM20–YSZ before thermal cycling, ●: LSF20–YSZ before thermal cycling, □: LSM20–YSZ after thermal cyclic treatment, ○: LSF20–YSZ after thermal cyclic treatment).

Table 1
The fitting parameters of LSM20–YSZ and LSF20–YSZ composite anodes at 1073 K.

Anode type	L (H cm^2)	R_s (Ω cm^2)	Q (Ω^{-1} cm^{-2} s^{-n})	n	R_{ct} (Ω cm^2)
LSM20–YSZ	8.44E-8	0.5769	0.02172	0.7133	0.236
LSM20–YSZ-2	1.469E-7	0.6058	0.007357	0.7629	0.3402
LSF20–YSZ	6.204E-8	0.5829	0.03855	0.6624	0.3020
LSF20–YSZ-2	1.831E-7	0.6199	0.01589	0.7585	0.4171

The equivalent circuit impedance was given as follow:

$$Z = j\omega L + R_s + \frac{1}{(1/R_{ct}) + (j\omega)^n Q} \quad (1)$$

The values of the parameters were illustrated in Table 1. The semicircle in EIS plot is associated with a charge transfer reaction at the electrode/electrolyte interface, which controls the oxidation of O^{2-} to O_2 at composite electrodes.

The polarization resistance R_p reflects the catalytic performance of the electrode [16]. It is equal to R_{ct} in case of single semicircle in this paper.

The results of EIS analysis showed that the polarization resistance of LSM20–YSZ was larger than that of LSF20–YSZ, which was consistent with the current density results. Meanwhile, after thermal cycling, the polarization resistances of both composite anodes were increased, which indicated the electrode degradation was caused by the reduction of triple-phase boundary during thermal cycling. It correlated well with the anodic polarization results. In addition, ohmic resistance R_s was slightly increased after thermal cycling. It might be caused by expansion differences between various materials during thermal cycling, which results in the increased contact resistance [17,18].

The electrochemical tests results show that LSF20–YSZ exhibits a better electrochemical catalytic behavior than LSM20–YSZ. It is more suitable to be applied in SOEC anodes.

4. Conclusion

Perovskite powders LSM20 and LSF20 were synthesized by sol–gel self-propagating method. The particle sizes of both powders were smaller than 50 nm. LSM20–YSZ and LSF20–YSZ composite anodes for SOEC were fabricated. Electrochemical performance measurements were carried out at 1073 K under electrolysis conditions. Compared to LSM20–YSZ, LSF20–YSZ exhibited a higher catalytic activity to the oxidation of O^{2-} to O_2. In addition, EIS analysis showed that the reduction of the anode performance after a complete thermal cycle was mainly caused by the degradation of the triple-phase boundary.

Acknowledgements

We would like to thank Dr. B. Yu, Dr. W.Q. Zhang, Dr. M.Y. Liu and Dr. M.D. Liang for their help in electrochemical performance measurements.

References

[1] G. Marban, T. Valdes-Solis, Int. J. Hydrogen Energy 32 (2007) 1625–1637.
[2] W.C. Lattin, V.P. Utgikar, Int. J. Hydrogen Energy 32 (2007) 3230–3237.
[3] S. Fujiwara, S. Kasai, H. Yamauchi, K. Yamada, S. Makino, K. Matsunaga, M. Yoshino, T. Kameda, T. Ogawa, S. Momma, E. Hoashi, Progr. Nucl. Energy 50 (2008) 422–426.
[4] Y. Shin, W. Park, J. Chang, J. Park, Int. J. Hydrogen Energy 32 (2007) 1486–1491.
[5] V. Utgikar, T. Thieesen, Int. J. Hydrogen Energy 31 (2006) 939–944.
[6] J.S. Herring, P. Lessing, J.E. O'Brien, Second Information Exchange Meeting on Nuclear Production of Hydrogen, Argonne National Laboratory, Illinois, USA, October 2003.
[7] J.E. O'Brien, C.M. Stoots, J.S. Herring, J. Fuel Cell Sci. Technol. 3 (2006) 213–219.

[8] J.S. Herring, J.E. O'Brien, C.M. Stoots, G.L. Hawkes, J.J. Hartvigsen, M. Shahnam, Int. J. Hydrogen Energy 32 (2007) 440–450.
[9] A. Hauch, S.H. Jensen, S. Ramousse, M. Mogensen, J. Electrochem. Soc. 153 (2006) A1741–A1747.
[10] S.H. Jensen, P.H. Larsen, M. Mogensen, Int. J. Hydrogen Energy 32 (2007) 3253–3257.
[11] J. Udagawa, P. Aguiar, N.P. Brandon, J. Power Sources 180 (2008) 354–364.
[12] J. Udagawa, P. Aguiar, N.P. Brandon, J. Power Sources 166 (2008) 127–136.
[13] M. Ni, M.K.H. Leung, D.Y.C. Leung, Int. J. Hydrogen Energy 32 (2007), 4648-466.
[14] W. Wang, Y. Huang, S. Jung, J.M. Vohs, R.J. Gorte, J. Electrochem. Soc. 153 (2006) A2066–A2070.
[15] M.D. Anderson, J.W. Stevenson, S.P. Simner, J. Power Sources 129 (2004) 188–192.
[16] J. Kong, K. Sun, D. Zhou, N. Zhang, J. Mu, J. Qiao, J. Power Sources 166 (2007) 337–342.
[17] Y.D. Zhen, J. Li, S.P. Jiang, J. Power Sources 162 (2006) 1043–1052.
[18] S.P. Jiang, J. Power Sources 124 (2003) 390–402.